

# Structure Through Colour: A Pixel Approach Towards Understanding Galaxies

M. M. Lanyon-Foster<sup>1\*</sup>, C. J. Conselice<sup>1</sup>, M. R. Merrifield<sup>1</sup>

<sup>1</sup> *University of Nottingham, School of Physics & Astronomy, Nottingham, NG7 2RD UK*

Accepted ; Received ; in original form

## ABSTRACT

We present a study of pixel Colour Magnitude Diagrams (pCMDs) for a sample of 69 nearby galaxies chosen to span a wide range of Hubble types. Our goal is to determine how useful a pixel approach is for studying galaxies according to their stellar light distributions and content. The galaxy images were analysed on a pixel-by-pixel basis to reveal the structure of the individual pCMDs. We find that the average surface brightness (or projected mass density) in each pixel varies according to galaxy type. Early-type galaxies exhibit a clear “prime sequence” and some pCMDs of face-on spirals reveal “inverse-L” structures. We find that the colour dispersion at a given magnitude is found to be approximately constant in early-type galaxies but this quantity varies in the mid and late-types. We investigate individual galaxies and find that the pCMDs can be used to pick out morphological features. We discuss the discovery of “Red Hooks” in the pCMDs of six early-type galaxies and two spirals and postulate their origins. We develop quantitative methods to characterise the pCMDs, including measures of the blue-to-red light ratio and colour distributions of each galaxy and we organise these by morphological type. We compare the colours of the pixels in each galaxy with the stellar population models of Bruzual & Charlot (2003) to calculate star formation histories for each galaxy type and compare these to the stellar mass within each pixel. Maps of pixel stellar mass and mass-to-light ratio are compared to galaxy images. We apply the pCMD technique to three galaxies in the Hubble Ultra Deep Field to test the usefulness of the analysis at high redshift. We propose that these results can be used as part of a new system of automated classification of galaxies that can be applied at high redshift.

**Key words:** Galaxies: Structure, Morphology, Classification, Evolution

## 1 INTRODUCTION

For as long as we have known about galaxies, astronomers have striven to classify them in a physically meaningful way. The long-standing method devised by Hubble (1926, 1936), with later revisions by de Vaucouleurs (1959) and Sandage (1961), has, until recently, been apt for this purpose. The Hubble sequence of morphological types is, on average, accurate for grouping together galaxies by structure and tells us about the typical distribution of stellar ages within a galaxy, as well as other properties (Roberts & Haynes 1994). However, classification is not an exercise to be carried out purely for its own sake; by classifying galaxies we hope to naturally obtain a picture of galaxy evolution. Furthermore, with the rapidly growing amount of data obtained at high redshifts, eyeball methods of classification are no longer viable, and the Hubble sequence breaks down for describing the galaxy pop-

ulation (e.g., Conselice, Blackburne, Papovich 2005, Conselice 2006b).

High redshift galaxies are also not adequately described by the Hubble sequence, as the majority of faint and/or distant galaxies are peculiar (Driver, Windhorst & Griffiths 1995, Driver et al. 1998, Abraham et al. 1996; Conselice et al. 2003, 2005, Lotz et al. 2006). At increasingly high redshifts, fewer and fewer galaxies appear to resemble nearby systems. Galaxy mergers, for example, become much more common at high- $z$  (e.g., Conselice et al. 2003; Lin et al. 2004; Cassata et al. 2005; Bundy et al. 2005; Conselice 2006; Bridge et al. 2007), and do not easily fit into any category of existing classification systems. Clearly, a new method of classification is needed that is physically meaningful and can naturally encompass and arrange all galaxy types, independent of redshift, that can be applied automatically to data with little or no human intervention.

Although the basic Hubble scheme has been revised and extended over the years to include increasingly complex mor-

\* E-mail: ppxmml@nottingham.ac.uk

phological structures within galaxies (e.g., de Vaucouleurs et al. 1959; van den Bergh 1960, 1995), these features are rarely seen at high redshift and do not account for the peculiar galaxies seen. A classification based on quantitative, objective indices are more suitable for classifying and quantifying these distant resolved galaxies.

The first attempt to develop such a scheme for nearby galaxies was made by Morgan (1958, 1959), who proposed a system based on a measure of the central concentration of light. This work has more recently been built upon by e.g., Bershady, Jangren and Conselice (2000), Conselice, Bershady and Jangren (2000) and Conselice (2003) who have extended this idea by developing the concentration, asymmetry and clumpiness (CAS) parameters. These parameters allow an extension of classification to objects over a wide range of redshifts and morphologies. However, these non-parametric indices do not utilise all the information presented in the resolved images of galaxies.

As such, we describe a new method of analysing the structures of galaxies on a pixel-by-pixel basis, based on similar method first used by Bothun (1986), Abraham et al. (1999) and Eskridge et al. (2003). Our approach is very general and we aim to determine how much information a pixel approach towards understanding galaxies reveals. We use photometric data to construct individual Colour Magnitude Diagrams of nearby galaxies such that each point corresponds to one pixel of a galaxy image. These pixel Colour Magnitude Diagrams (pCMDs) are used to examine the stellar populations and structure of the galaxies and we discuss ways this technique can be applied at high redshift.

We find that pCMDs provide information about galaxy morphology, in particular early-type galaxy pCMDs are very different to those for late-type galaxies. The pCMDs can be used to pick out individual features and this has led to the discovery of ‘‘Red Hooks’’ in six early-type galaxies. We find that quantitative parameters can be obtained from pCMDs, which can potentially be used as measures of classification. Comparisons to stellar population models can also be made on a pixel-by-pixel basis, presenting a new perspective on galaxy structure and evolution. We show that pixel-by-pixel analysis can be applied to high redshift galaxies and this is briefly tested on three Hubble Deep Field galaxies.

The pCMD method is explained and the sample is defined in §2. The resulting pCMDs are presented and the main trends found are detailed in §3, and individual cases are examined. A quantitative analysis of pixel light and colour is made in §4 and comparisons to stellar population models are made in §5. An application of the pCMD method is made to 3 UDF galaxies in §6 and our conclusions are discussed in §7.

## 2 THE DATASET AND METHOD

It is essential in any work on galaxy classification that a wide range of Hubble types are considered. It is primarily for this reason that we select the Frei et al. (1996) sample of nearby galaxies for this study. This is a digital multiband sample of 113 local galaxies, made up of CCD images taken from observations at the Lowell and Palomar Observatories. The galaxies in this sample are all bright and well resolved, which is necessary for a structural study such as this.

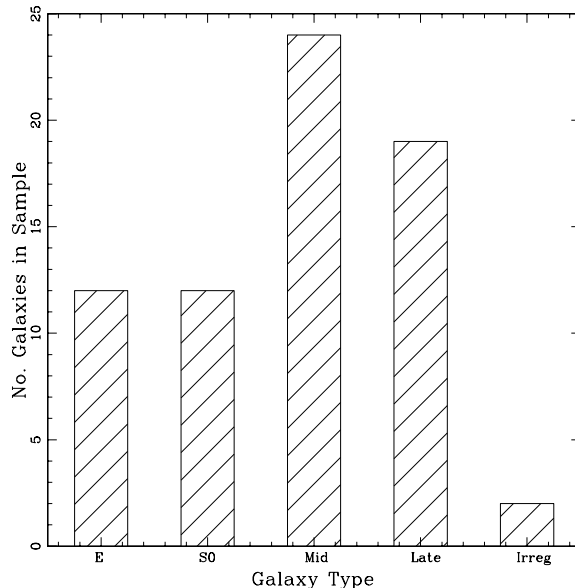


**Figure 1.** The distribution of galaxy types in the sample.

Images obtained at the Lowell observatory are available in  $B_J$  (450nm) and  $R$  (650nm) bands whereas the Palomar galaxies are obtained in  $g$ ,  $r$ , and  $i$  bands of the Thuan-Gunn photometric system. Our sample is refined to the 82 Lowell images so that the colours of the galaxies can be accurately compared. We remove 13 of the 82 galaxies from the sample due to low signal-to-noise. Figure 1 illustrates the distribution of galaxy types in the sample.

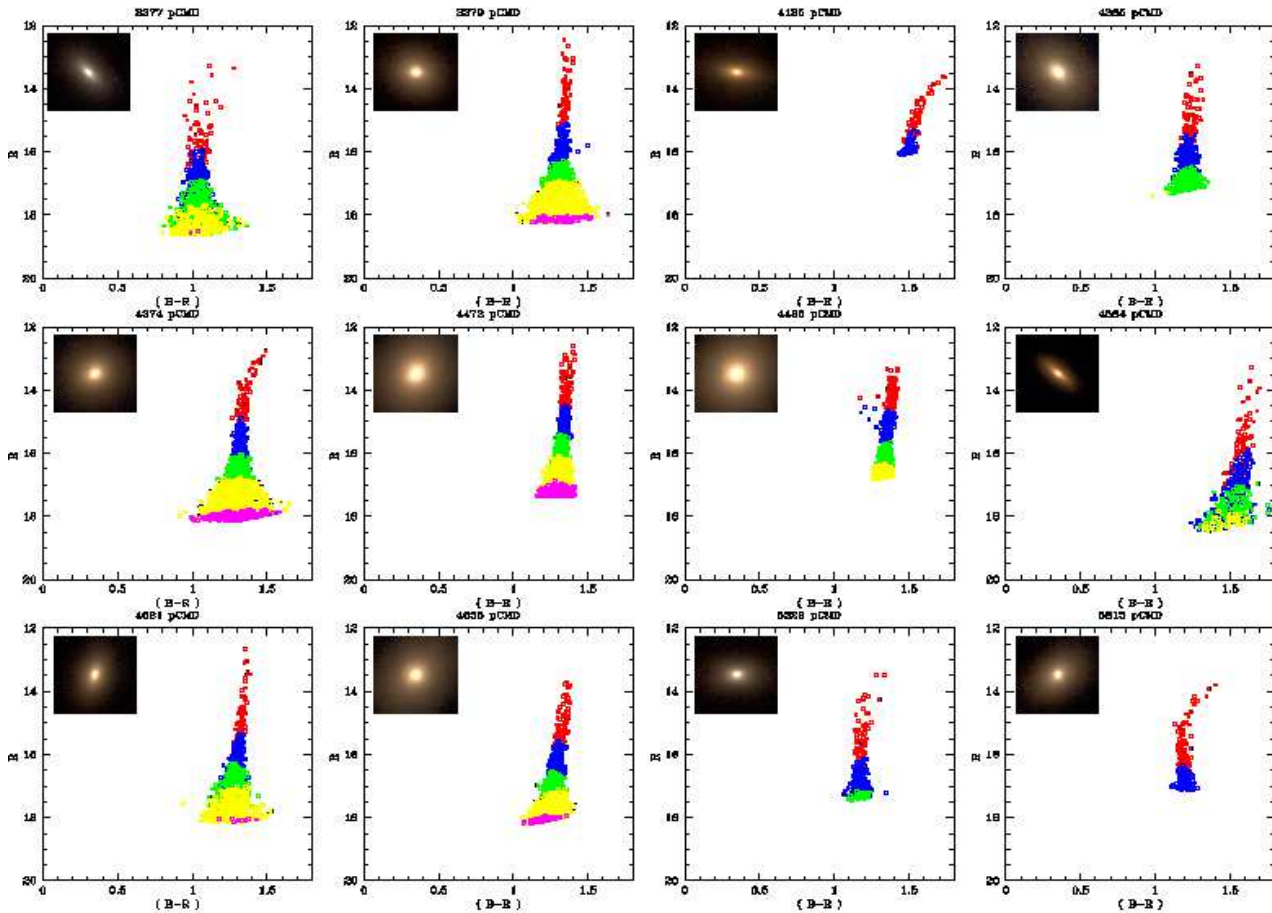


**Figure 2.** The pCMDs of the elliptical galaxies in the sample. Each galaxy is displayed in its own pCMD and are colour coded by radius. Radius limits were set at 5, 10, 15, 25, 35 and 50 pixels from the centre, corresponding to the red, blue, green, yellow, magenta, cyan and black data points respectively.

The pCMDs are computed through the manipulation of the  $B_J$  and R band galaxy images using the Image Reduction and Analysis Facility (IRAF). The background sky value is subtracted from all images. The centres of the images are found and the R band images shifted such that the pixels are aligned with those of the corresponding  $B_J$  band image. Pixel alignment is crucial in this method and we are able to match our images to an accuracy of  $\pm 10^{-5}$  pixels.

The original pixel scale of the images in our subset of the Frei sample is 1.35 arcsec per pixel. The typical seeing for these galaxies is between two and four arcseconds. In order to obtain a pixel scale that is at least on the order of the PSF, we bin the the images by a factor of two. This ensures that each binned pixel is statistically independent of the surrounding pixels and improves the signal-to-noise.

Corrections are made for galactic extinction using values obtained from the NASA/IPAC Extragalactic Database (NED) and a cut is made at a signal-to-noise ratio of two. Fluxes are converted from counts per pixel to apparent magnitude per square arcsecond by considering the pixel scale. Absolute magnitudes are calculated using distances to the galaxies, which are taken from Conselice et al. (2000). The  $(B_J - R)$  colour index is calculated from each pixel in the image and values for each galaxy are plotted on a separate pCMD.

Each galaxy is plotted on its own Colour Magnitude Diagram (CMD), with each point on the CMD corresponding to one pixel of the galaxy image. The points are colour-coded according to distance from the centre of the galaxy. The red data points are the most central, falling within a radius of 5 pixels from the centre of the galaxy. Radius limits are then set at 10, 15, 25, 35 and 50 pixels from the centre, corresponding to the blue, green, yellow, magenta, cyan and black data points respectively.

The pixel Colour Magnitude Diagrams (pCMDs) represent a method of illustrating the structure of a galaxy through its CMD. Indeed, we have found that the shape of a galaxy’s pCMD is strongly correlated to its morphology and Hubble type. This will be explained in detail in Section 3.

We construct pCMDs for 69 galaxies in total, comprising of: 12 elliptical galaxies (Figure 2), 12 S0s (Figure 3), 24 mid-types (Figures 4 & 5), 19 late-types (Figure 6) and 2 irregular galaxies (Figure 7). Throughout this paper we define early-type galaxies as both elliptical and lenticular, mid-type galaxies as those on the sequence Sa-Sb(c) and late-types as those on the sequence Sc-Sd(m). The classifications of Conselice et al. (2000) are used throughout.

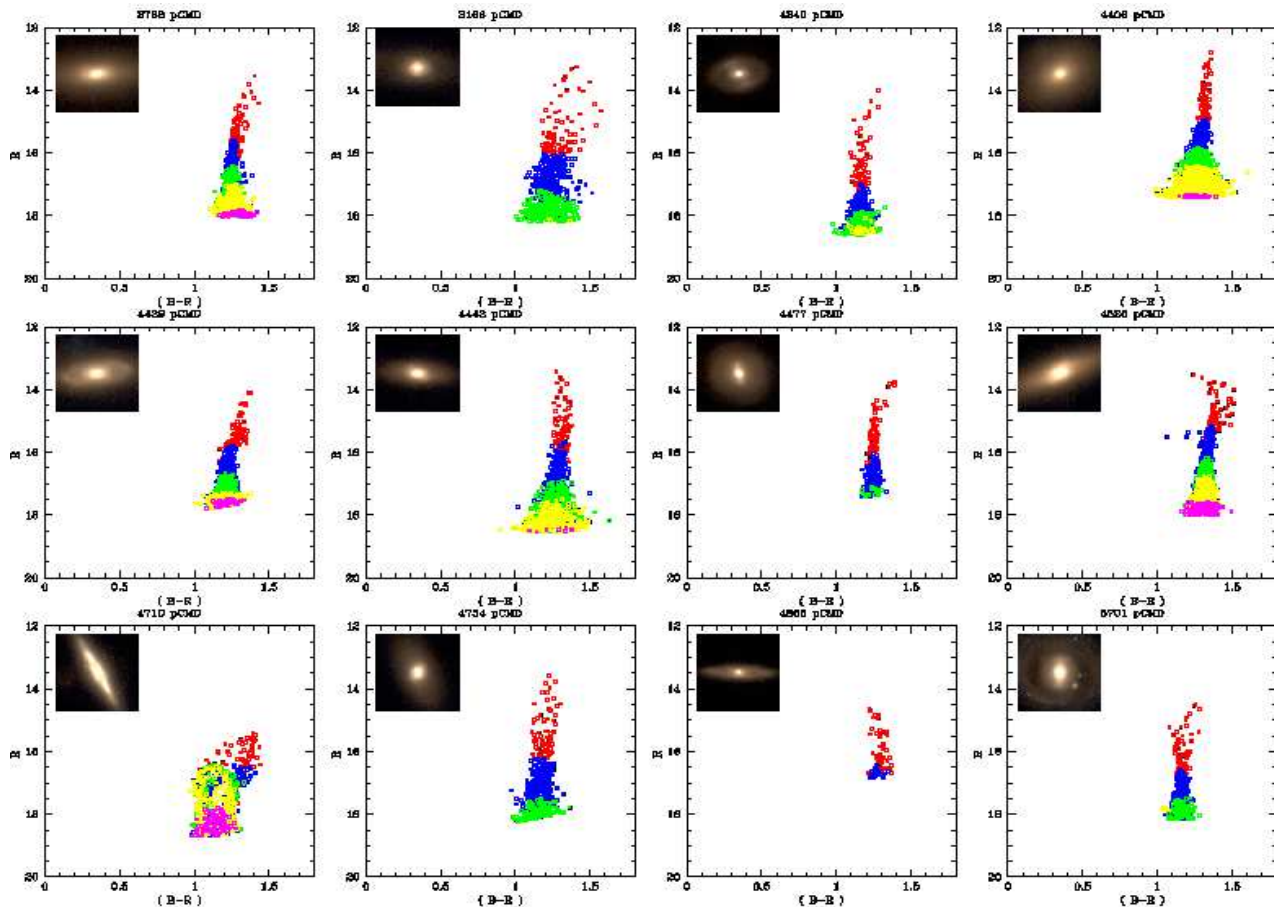


**Figure 3.** The pCMDs of the S0 galaxies in the sample. The colour coding of the pixels is the same as in Figure 2.

### 3 MAIN TRENDS

The pCMDs (Figures 2-7), despite appearing to vary widely, tend to have similar features when sorted by galaxy type. In this section we will discuss the various forms of the pCMDs and the trends found across the Hubble sequence.

#### 3.1 Early-Type Galaxies

##### 3.1.1 Elliptical Galaxies

The pCMDs of the ellipticals (Fig. 2) all have very similar qualities. They all have pixel colours of  $(B - R) \geq 1$  and display a narrow “prime sequence” between colour and magnitude. We define this prime sequence as a narrow trend between pixel colour and magnitude such that pixels that are brighter are also redder. The spread in colour of the ellipticals tends to be small throughout the radius of the galaxy, the average colour dispersion at a fixed magnitude being  $0.029 \pm 0.014$  (see §4.3). This is expected for the ellipticals and is explained by their structure and homogeneous age. They are old systems with mature stellar populations and little or no current star formation (e.g. Bower et al. 1998).

##### 3.1.2 S0s

The S0 sample (Fig. 3) yielded pCMDs with properties resembling those of the ellipticals but with some subtle dif-

ferences. The spread of colour of the pixels throughout the radii of the S0s appears slightly larger than that of the ellipticals in most cases, the average colour dispersion at a fixed magnitude being  $0.036 \pm 0.019$  (see §4.3). This is likely to be accounted for by considering that S0 galaxies tend to be dustier systems than elliptical galaxies and such a spread in colour of pixels located at the same radius in the galaxy appears to be strongly influenced by the presence of dust in the galaxy (see §3.2.1 & §3.3.3).

S0s are also well known to have bluer disks than bulges (e.g., Bothun & Gregg 1990). This stellar population/metallicity effect could also potentially account for the larger colour dispersion at a fixed magnitude in the S0 pCMDs.

This phenomenon could be of use in separating Es and S0s, a notoriously tricky feat to accomplish by eye alone. It is possible that S0s with a tight prime sequence may in fact be misclassified ellipticals (e.g. NGC 4406, Fig. 3) and vice versa for those ellipticals with a large uniform spread (e.g. NGC 3377 & NGC 4564, Fig. 1). However, this assertion will need to be tested on a larger sample of early-type galaxies before it can be made with any certainty.

#### 3.2 Mid to Late-Type Galaxies

The mid and late-type galaxy (Sa-Sd) pCMDs differ from the early-types. There are general trends amongst these

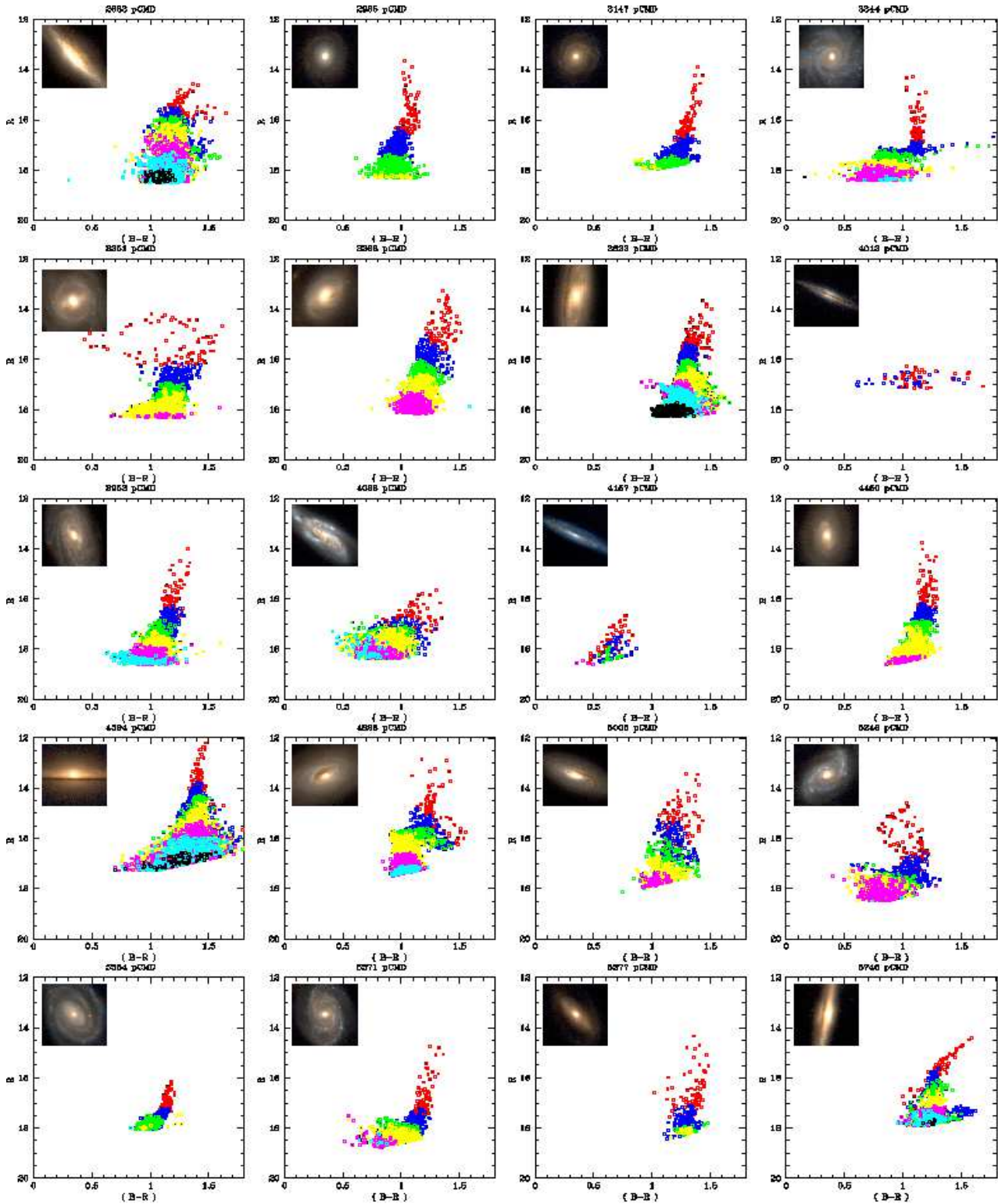


Figure 4. The pCMDs of the mid-type spiral galaxies in the sample. The colour coding is the same as in Figure 2.

classes, such that the average position on the pCMD is bluer than the early-types and has a larger colour gradient. The pixel colour coding shows that the inner pixels of these galaxies are the reddest, with  $(B - R)$  decreasing with increasing radius. The spread in colour is largest in the outer parts of the galaxy. There is also a larger spread in the inner

regions of the spirals than for the early-types. Out to a five pixel radius (red points in Figures 2-7) the average colour spread for the spirals is  $0.38 \pm 0.20$  magnitudes. In the same region in the early-types the average spread is  $0.21 \pm 0.10$  magnitudes.

Mid and late-type galaxy pCMDs are also not as uni-

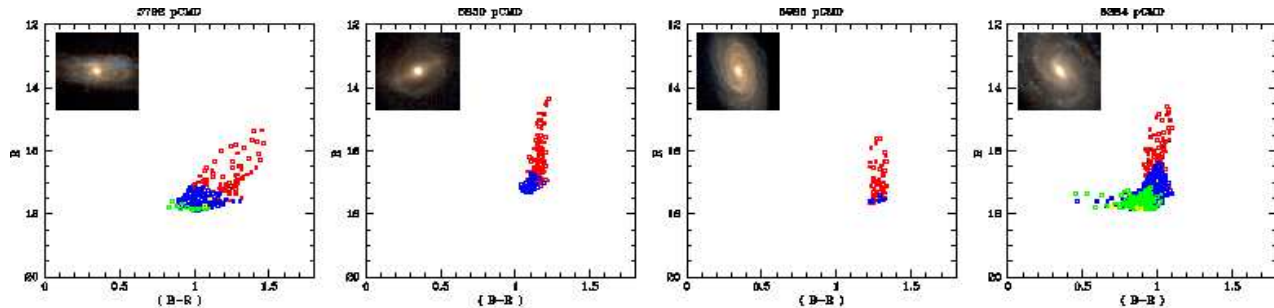


Figure 5. The pCMDs of the mid-type spiral galaxies in the sample continued.

form as those of the early-type galaxies (Figs. 4-6). There are, however, some striking correlations between the shape of the pCMD and the physical properties of the galaxies.

### 3.2.1 Dusty and High Inclination Spirals

pCMDs with a large spread in colour throughout the radius of the galaxy are found to correspond to systems with a high inclination angle and dust content. NGC 3079 (see Fig. 6) is a typical example of how much effect the inclination of a galaxy can have on its pCMD. Star formation can be seen in the outer edge of the disk, where the pixels are bluest. There is a colour gradient similar to other mid and late-types but there is also more spread in colour at all radii. That is, the prime sequence is not well defined for these galaxies.

There is a definite correlation between dust features in the galaxy image and colour spread in the pixels (see §3.3.3). It is evident that dust can block light altogether if it is dense enough. In the pCMD of NGC 4013 (Fig. 4) the brightest light in the bulge of the spiral is absorbed by the prominent dust lane that runs the length of the spiral and is most noticeable due to the very high inclination of the galaxy.

### 3.2.2 “Inverse-L” Shapes

Some pCMDs are found to have abrupt changes in colour rather than a continuous gradient. Such “inverse-L” shapes are found to correspond to face-on spirals. The inner pixels appear very similar to typical elliptical pCMDs with a prime sequence, while the outer pixels suddenly become much bluer. Such behaviour is naturally explained by an old, red bulge surrounded by blue, star-forming spiral arms. NGC 3344 (Fig. 4) clearly exhibits this structure.<sup>1</sup>

## 3.3 Individual Cases

Unusual features are picked out in some of the pCMDs. For example, in some cases pixels that deviate from the main

trend are found to correlate with physical features of the galaxy. We discuss here some of the unusual pCMD features that are discovered and explain them in terms of the structural and physical properties of the galaxies.

### 3.3.1 Central Red Pixels - The “Red Hooks”

We find that in the very central regions of 8 galaxies the colour gradient of the pixels suddenly become much redder with decreasing magnitude than the outer regions of the galaxy. These red pixels are, on average, within a radius of 2.5 pixels, or approximately 300pc, from the centre of the galaxy. These galaxies are NGC 4125, NGC 4374, NGC 5813, NGC 2768, NGC 4340, NGC 4477, NGC 5746 and NGC 3631, which comprise 3 ellipticals, 3 S0s, 1 mid-type and 1 late-type spiral, respectively and can be found in the corresponding figures.

It is not unknown for some ellipticals to have colour gradients such that their central regions are substantially redder than their outskirts (e.g. Binney & Merrifield, 1998). Here we investigate the emergence of this effect in a pixel-by-pixel context. The luminosities of these galaxies are compared with those of the rest of the sample using values quoted in Conselice et al. (2000). All eight galaxies are bright but have luminosities typical of the sample, in the range  $-19.17 \leq M_B \leq -21.73$ .

A likely cause of the Red Hooks is dust reddening. In a study of 77 early-type galaxies, Lauer et al. (2005) found that dust was present in the central regions of about half of their sample. This is on a similar scale to that which the central red pixels (CRPs) in the Frei sample are found, although a much higher resolution was available in the HST/WFPC2 images. Nine of our early-type galaxies are in both the Frei and Lauer et al. samples, three of which are identified as having central red pixels. On the whole we find that galaxies with no central reddening in our sample contain little or no dust, whereas those identified as Red Hooks have visible dust structures obscuring the central part of the galaxy, as identified from the Lauer et al. study. This strongly suggests that dust is a major factor in causing the Red Hook phenomenon. It is proposed by Lauer et al. that the dust features that they have observed may outline gas that is falling into the central black hole of the galaxy.

In general, those galaxies which appear to be very dusty in their images tend to show a larger dispersion in  $(B - R)$  colour in their pCMDs, as opposed to the neatness of the Red Hooks. However, if these dust features exist in the central regions of early-types, the orientation of such structures

<sup>1</sup> The odd branch of pixels that can be seen in the pCMD of NGC 3344, which appears much redder than others at the same radius, correlates with a foreground star that was removed in the B band image but not in the R band. This demonstrates that unusual features in the pCMD do correspond with a real feature, in this case a data reduction oversight. We discuss in §3.3 some examples where physical structures within the galaxy have been detected in the pCMDs.

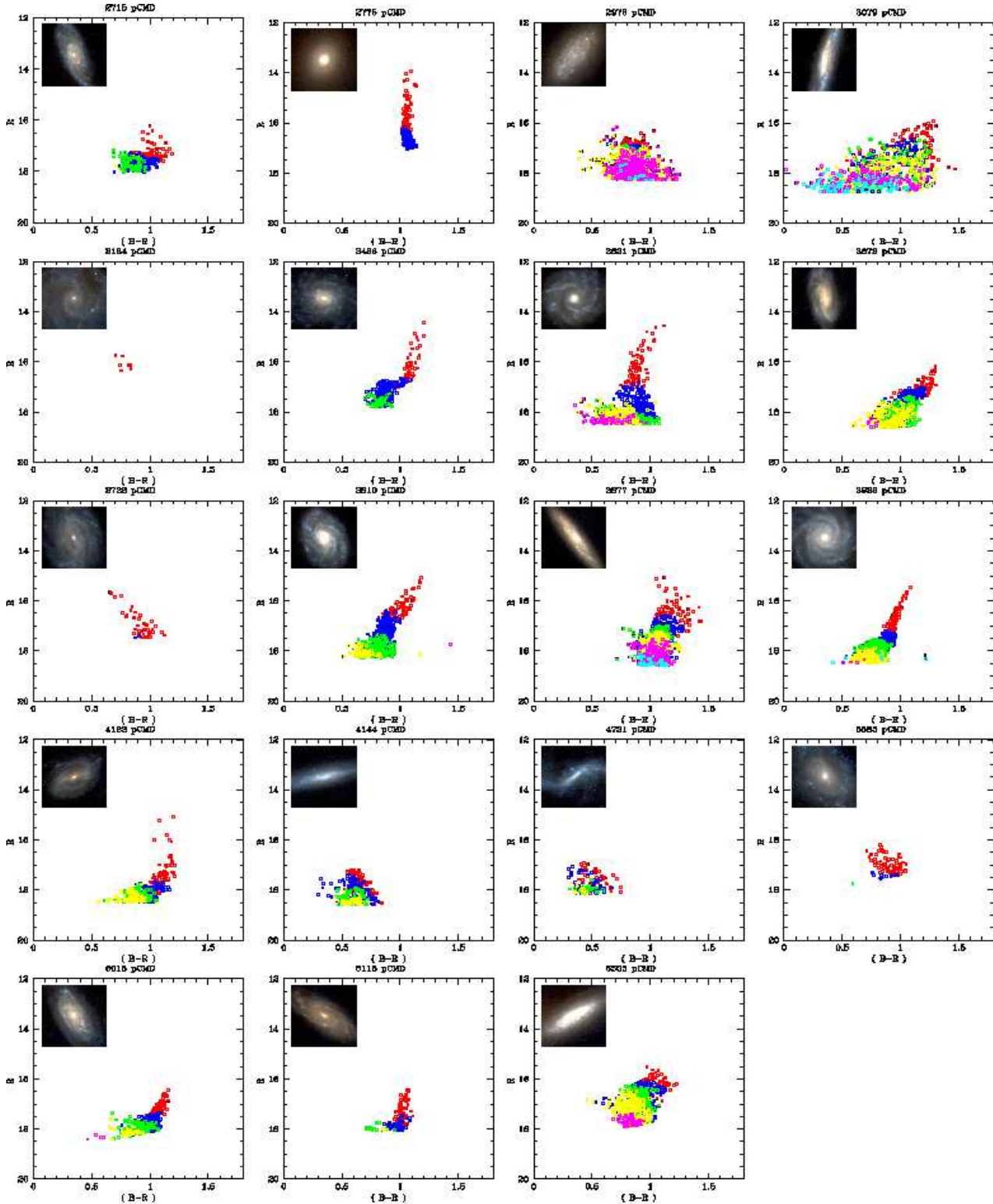
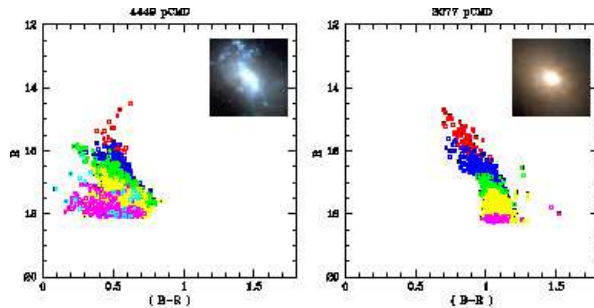


Figure 6. The pCMDs of the late type spiral galaxies in the sample. The colour coding is the same as in Figure 2.

and the amount of dust that is concentrated in the small central region may have a different effect on the pCMD than large scale dust lanes. The observed orientation of the dust rings and the amount by which they obscure the nucleus of the galaxy could also influence the resulting pCMD. Al-

though this is an attractive idea, a more extensive and detailed study of this topic is required.

We also investigated whether the Red Hooks could be produced by AGN. Of the eight galaxies that show this central reddening effect, six have known AGN activity. Ho et al.



**Figure 7.** The pCMD of the irregulars in the sample, NGC 4449 and NGC 3077. The colour coding is the same as in Figure 2.

(1997) studied a sample of more than 200 nearby galaxies and classified their cores via spectroscopic measurements, including 56 of the galaxies in our sample. Of the three elliptical galaxies found to have this central reddening effect, NGC 4374 and NGC 5813 are both classified as L2 type LINER cores whilst NGC 4125 is classified as a T2 transition object. According to the arguments of Ho et al., transition objects are most naturally explained as being “normal” LINERs whose spectra are diluted or contaminated by neighbouring HII regions. Thus all three elliptical galaxies with a reddening of their central pixels belong to the LINER class of galaxies.

Of the three S0s to show this effect, NGC 2768 is also classed as an L2 LINER galaxy whilst NGC 4477 is classed as an S2 Seyfert galaxy. No information is available for NGC 4340. NGC 5746, a mid-type spiral, is also classed as a T2 transition object whereas NGC 3631, a late-type spiral, has a HII core.

It is thus possible that interactions between the AGN and the interstellar gas in the inner regions of these galaxies could affect the colours in these regions. At least 34 out of the 69 galaxies in our sample are thought to have some form of AGN activity, however, only six of them display the central reddening effect.

A similar effect to the Red Hooks has been observed by e.g., Cantiello et al. (2005), who looked at surface brightness fluctuations and colour gradients of elliptical galaxies in the B and I bands. They also observed a steepening in the (B-I) colour gradient in the centres of three elliptical galaxies. Such colour gradients could provide a tool for investigating galaxy formation.

The fact that this steepening of the colour gradient is observed to occur in only eight of the 69 galaxies analysed suggests that not all galaxies have identical formation histories and/or properties, even within the early-types. It is evident that this effect appears to be mostly associated with early-type galaxies. This could imply that the central steepening of the colour gradient is a phenomenon that emerges with time.

### 3.3.2 NGC 4486 (M87) - AGN

The pCMD of M87 (Figure 8) contains a branch of pixels that are bluer than most other pixels at the same radius. These pixels are traced to a physical region in the galaxy that appears as a bright spot, which is a manifestation of the optical jet that originates from the central black hole of

M87. This jet is formed within a few tenths of a light year of the galaxy’s core (Junor et al. 1999).

### 3.3.3 NGC 4826 - Extreme Dust

The pCMD of NGC 4826 (Figure 9) is unlike any other observed. The inner pixels of the image appear to split into two branches clearly separated in both colour and magnitude. The fainter, redder branch when physically mapped is revealed to correspond to a region above the central bulge of the galaxy where there is a prominent dust lane. Without this feature, the pCMD of NGC 4826 would be typical of a mid-type galaxy.

## 4 QUANTIFYING PCMD STRUCTURE

Through analysis of the information that can be gained from the pCMDs, we construct new parameters formulated to pick out more fundamental properties of galaxies and hence lead to a new, objective classification system. We explore a number of such methods, including the pixel blue-to-red light ratio and colour spread, which we detail below.

### 4.1 Average Colour Magnitude Diagram

The average pixel colour and magnitude for each galaxy is calculated by considering each pixel of the galaxy image. These average values for each galaxy are plotted in Figure 10. We see a trend such that the early-types are brighter and redder than the spirals. In turn, the mid-types tend to be redder and brighter than the late-types. This points to a natural evolution along the Hubble sequence and is not unexpected.

This is a surface area weighted average as all pixels are summed independently, without being given a weighting according to how bright they are. Using a lower value for signal-to-noise has the effect of raising the total R brightness value but the average (B-R) colour stays approximately the same. Therefore, using a lower cut-off for surface brightness will have the affect of shifting the relation up slightly, in approximately the same manner for all galaxies. For a higher S/N, the colour will stay approximately the same but the average R value will be lower.

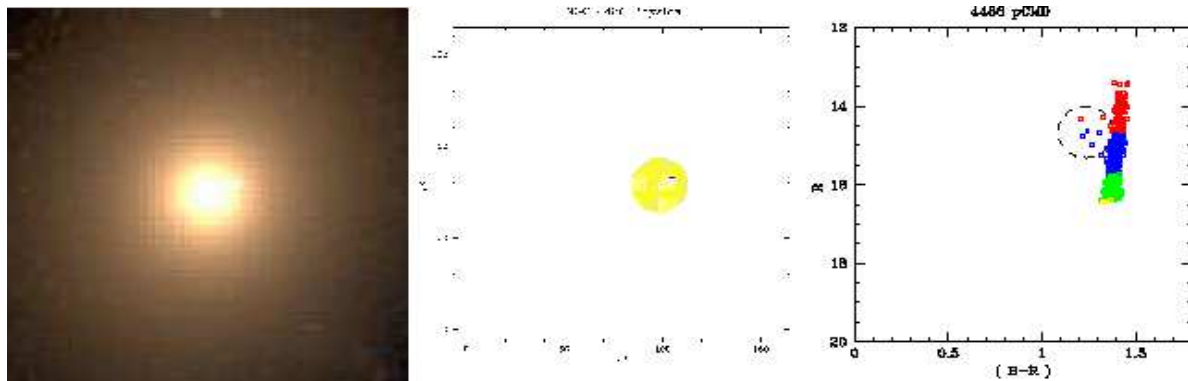


**Figure 8.** A physical mapping of the blue branch of pixels in NGC 4486 (M87). The image of NGC 4486 on the left is taken from the Frei et al. (1996) catalogue. The central image shows a physical plot of the galaxy (yellow pixels) with the blue branch of pixels overlotted in their corresponding colours, circled in the pCMD to the right. The few pixels that appear bluer than the main trend are shown to correspond to the optical jet of M87.

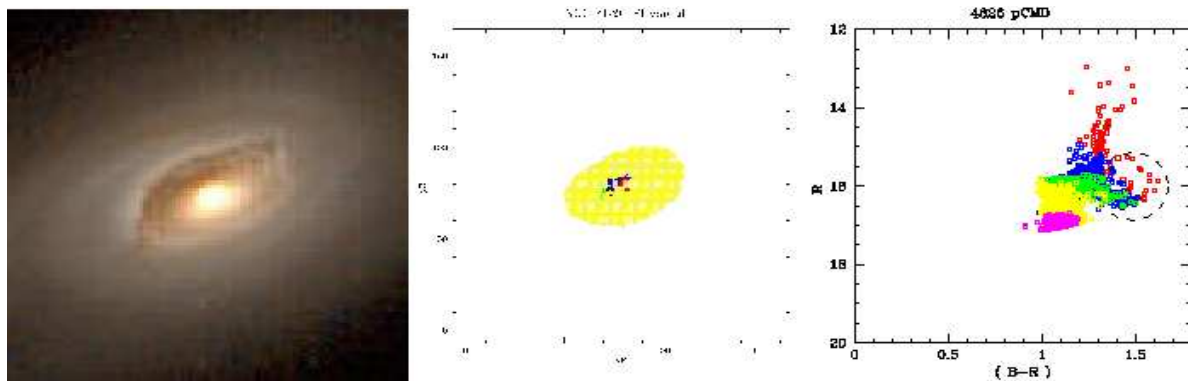


**Figure 9.** A physical mapping of the red branch of pixels in NGC 4826. The central image shows a physical plot of the galaxy (yellow pixels) with the red branch of pixels overlotted in their corresponding colours, circled in the pCMD to the right. The fainter, redder branch of pixels in the pCMD is shown to correspond to the prominent dust lane above the central bulge.

## 4.2 Fitting the pCMDs

We fit straight lines to the prime sequences of the pCMDs for most of our galaxies, taking into account the error due to enhanced noise at low brightnesses. The pixels in each galaxy are binned into intervals of two pixels in radius. The average colour and the average colour dispersion within each of these intervals are then calculated and plotted.

These fits are a good representation of the behaviour we find in the pCMDs of early-type galaxies but are obviously a poor representative of spiral and irregular galaxies. The pCMDs of mid and late-type galaxies cannot be characterised by such a simple functional form. The slopes tend to be steeper for early-type galaxies but there is no clear pattern to distinguish ellipticals from lenticulars. The irregular galaxies, NGC 3077 and NGC 4449 (Fig. 7), possess slopes that are opposite in sign to the early-types and spirals due to the fact that they are bluest in their inner regions.

An example of each galaxy type is shown in Figure 11. Straight lines are fit to all except the late-type spiral, NGC 3631, which clearly cannot be described by such a fit. We note that the spread in colour of the S0 (NGC 3166) is larger than the elliptical (NGC 4472) and is more or less constant throughout its radius. This confirms the observations noted in §3.1.2.

## 4.3 Investigating the Average Colour Dispersion

### 4.3.1 Average Colour Dispersion Vs. Inclination Angle

To test the relationship between dust content of a galaxy and spread in colour in the pCMD, the average colour dispersion of the galaxy is compared with the inclination (Fig. 12). The average colour dispersion for each galaxy is calculated by taking the mean of the spread in radial intervals as defined in §4.2. The inclination angles are obtained from the online Frei catalogue (1996). This test is limited to the mid and late-type spirals in the sample so as to avoid any errors due to misclassification in the S0s.

In Fig. 12 the late-type spirals are plotted as blue triangles and the mid-types as green hexagons. Despite the scatter in the plot, there is clearly a positive trend between the average colour dispersion and inclination angle of a galaxy. This implies that highly inclined galaxies are more likely to have a large spread in colour in their pCMDs, and the greater the inclination, the higher the internal spread in colour. This is evidence in favour of the idea that a large scatter in colour in the pCMDs is partially due to the influence of dust. However, we recognise that the colour dispersions are not caused solely by dust, they are also influenced by differences in stellar populations within the galaxy.

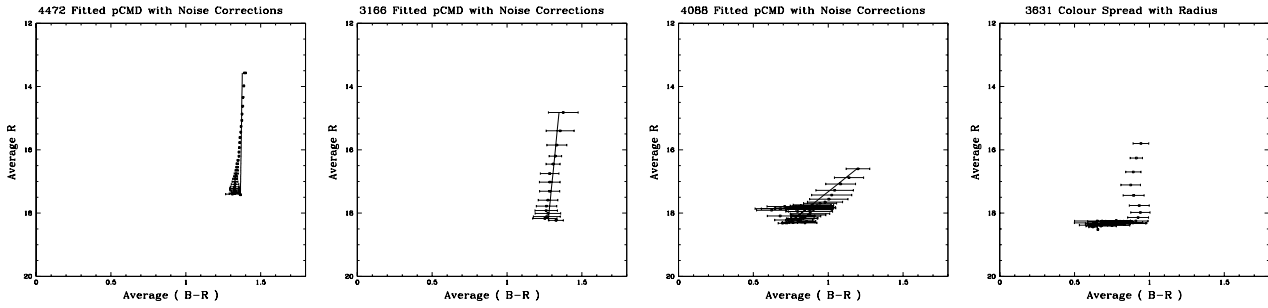


**Figure 11.** Examples of the fits to the pCMDs. Above, from left to right, are NGC 4472 (E), NGC 3166 (S0), NGC 4088 (mid-type) and NGC 3631 (late-type). The points represent the average (B-R) colour and the error bars represent the 1 sigma scatter in colour at various magnitudes. While a straight line fit works well for the early-types, it cannot be used to characterise the spirals.

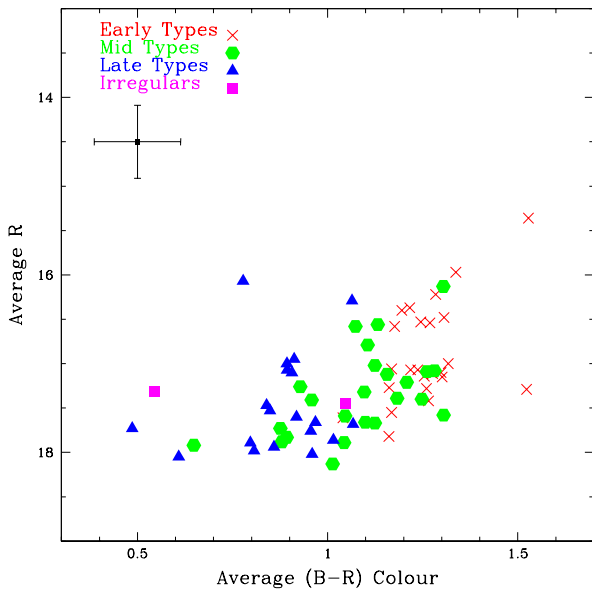


**Figure 10.** The average colour magnitude diagram of the sample. Each point corresponds to the average colour and brightness of one galaxy, calculated on a pixel-by-pixel basis. The early-types are represented by diagonal crosses, mid-types by hexagons, late-type by triangles and the irregulars are shown by square points.

To test this idea, we compare the residuals of the inclination-average colour dispersion fit (Fig. 12) with the average colour of the galaxies to check for any systematic effects due to colour. We find no significant correlation, which indicates that the scatter in the inclination Vs. colour relation is not produced by differences in star formation histories.

#### 4.3.2 Average Colour Dispersion Vs. Average Colour

We plot the average pixel (B-R) colour of each galaxy (as calculated in §4.1) against the average colour dispersion (Fig. 13). We include the early-type galaxies of the sample in this plot, represented by the red crosses. There is a large scatter but there is a trend for redder galaxies to have a lower average colour dispersion. There also appears to be a clear separation in the average colour dispersion of early and late-

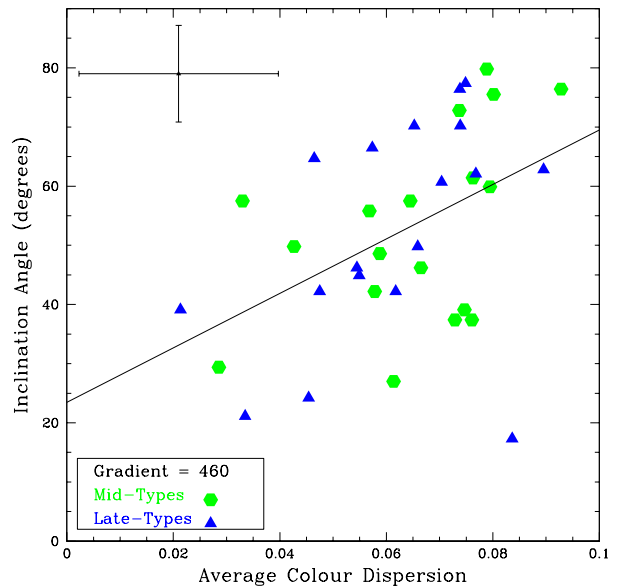


**Figure 12.** The average dispersion in colour of each galaxy is plotted against inclination angle, as given in the Frei catalogue. Mid-type and late-type galaxies are plotted as green hexagons and blue triangles, respectively. A positive correlation can be distinguished but there is no discernable difference between the mid and late-types.

type galaxies at around 0.05. This could imply a fundamental difference between galaxies with star formation present and those without.

The late-type galaxy that has a particularly red colour and low dispersion for its type is NGC 2775 (Fig. 6), which has a particularly faint disc compared to the brightness of its central bulge. After signal-to-noise cuts only the inner radius of 10 pixels from the galaxy centre remains, which corresponds to only bulge light, giving the galaxy similar properties to that of an early-type in this analysis. It is also possible that NGC 2775 could be misclassified as a mid-type.

## 4.4 Blue-to-Red Light Ratio

A central theme that emerges from the pCMDs is the fact that different galaxies have different colour distributions and

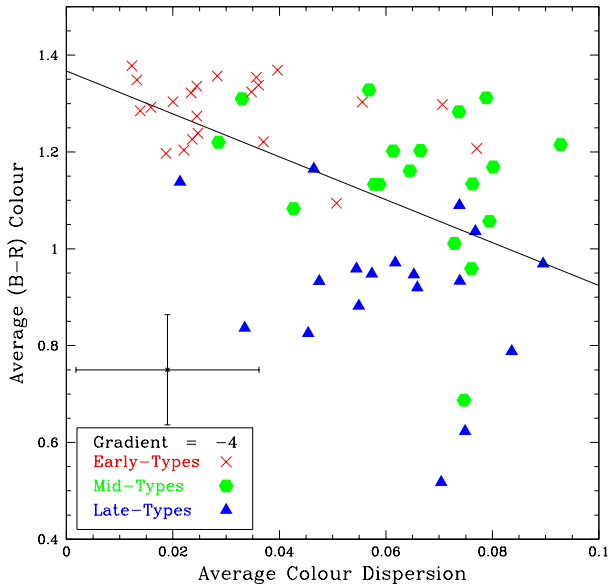


**Figure 13.** The average (B-R) colour of each galaxy is plotted against the average dispersion in colour. Early-type galaxies are included in this plot and are plotted as red crosses. There is a trend for the redder galaxies to have a lower average colour dispersion. Late-type galaxies are distinguished from early and mid-types due to their blue colours.

these are related to morphological type. This is not a new idea, as it is well known that early-type galaxies tend to be redder systems than late-type spirals, which are hosts to star formation. The analysis of bulge-to-disc ratios is another useful measure of the properties of spiral galaxies, as found by Driver et al. (2006). Analogous to this concept, we note that the ratio of total blue to total red light in a galaxy could be a useful way of distinguishing between galaxy types. We propose a new parameter to quantify this, the blue-to-red light ratio.

A cut is made at  $(B - R) = 1$ , such that pixels with colours above that value are defined as red light and those with colours below this value are defined as blue light. In the Padova (1994) stellar population models with a Chabrier IMF (Bruzual & Charlot, 2003), which will be used in a further analysis later on,  $(B - R) = 1$  corresponds to an age of 1 Gyr. This is the age at which metallicity effects become important in colours, thus making  $(B - R) = 1$  an appropriate cut. The blue-to-red light ratio for each galaxy is defined as the difference between the total blue light and the total red light contained in the pixels, divided by the total light. This gives a spatial measure of the colours in the galaxy without being dependent on the intrinsic brightness of the galaxy itself. We define the blue-to-red light ratio to be:

$$\frac{N_B - N_R}{N_B + N_R} = \frac{\sum_{n=1}^N p_n |_{(B-R) < 1} - \sum_{n=1}^N p_n |_{(B-R) > 1}}{\sum_{n=1}^N p_n} \quad (1)$$

Where  $N_B$  is the total number of pixels below the  $(B - R) = 1$  cut,  $N_R$  is the total number of pixels above it,  $N$  is the total number of all pixels and  $p$  represents each pixel in the galaxy image.

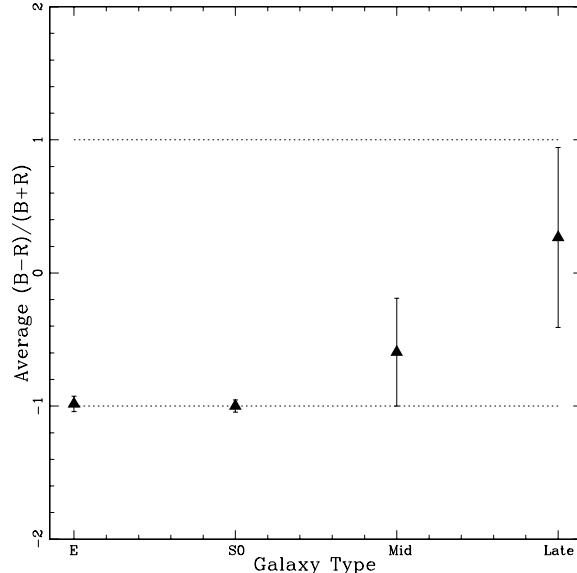


**Figure 14.** The average blue to red light ratio for each galaxy type.

Figure 14 shows the average blue-to-red light ratio for each galaxy type: E, S0, Spirals and Irregulars. A clear positive correlation can be seen, with elliptical galaxies on average composed of mostly red light and the amount of blue light contained in a galaxy increasing for later Hubble types. The blue-to-red light ratio can be used to sort galaxies into early or late-type and this could be an appropriate measure when looking at irregular structures at high redshift.

#### 4.5 Galaxy Colour Distributions

Figure 15 shows the cumulative distribution of colour for all galaxy types, taking each pixel into account. There is almost no overlap in colour between elliptical galaxies and late-type spirals, whereas the mid-type and S0 peaks lie between these with significant overlap. There appears to be a natural progression in colour from late-type (blue) to early-type (red) along the Hubble sequence.

It is interesting to compare this plot to the work of Driver et al. (2006) who examined bulge-disc compositions of early-type spirals. Driver et al. see a clear separation between the bulge and disc of early-type spirals, with bulges occupying their “red compact peak” and discs their “blue diffuse peak”. However, the S0 colour distribution in Fig. 15 significantly overlaps with the elliptical and mid-type colour distributions and hardly at all with the blue, late-type distribution. This implies that the bulges of lenticular galaxies are as red (or redder, perhaps due to dust) than some pixels of elliptical galaxies but there is no clear blue peak of pixels relating to the S0 disc component.

We also do not see clear and distinct bulge and disc colour bimodality in a pixel analysis of  $(B - R)$  colour distribution for mid or late-types. There appears, rather, to be a steady sequence in colour across each galaxy type.

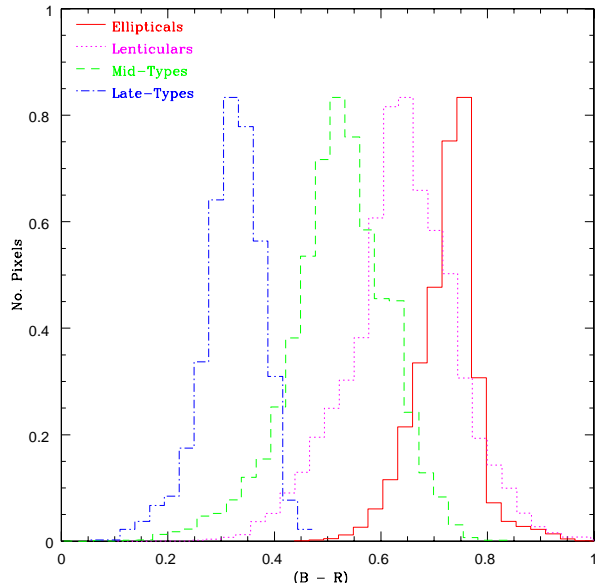


**Figure 15.** The total colour distributions for pixels, sorted into galaxy types.

## 5 COMPARISON TO STELLAR POPULATION MODELS

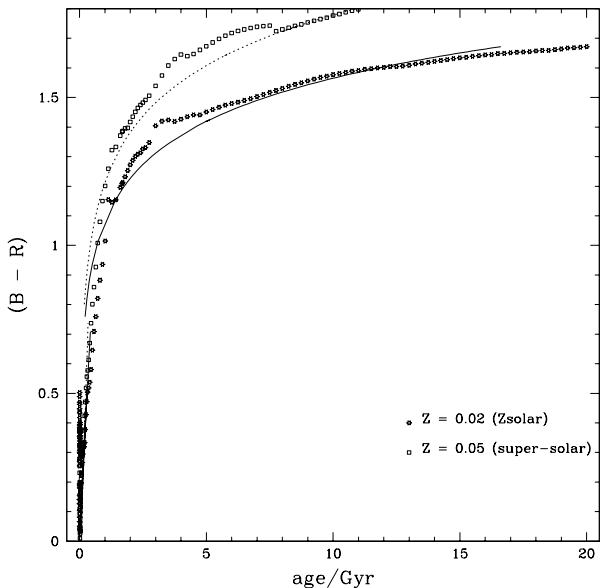
We use the stellar population models of Bruzual & Charlot (2003), hereafter BC03, to obtain very rough relative age estimates of the pixels in each galaxy. We use the Padova (1994) model with a Chabrier IMF. The available metallicities in these models are sub-solar, solar and approximately twice solar. None of the galaxies in our sample are likely to be sub-solar, on average, as they are all massive and luminous. It is also impossible to calculate metallicities on a pixel-by-pixel basis with only two photometric bands. Therefore, for this preliminary analysis and for comparison purposes, solar metallicity is used for all pixels. We do, however, recognise that internal galaxy metallicity gradients are ignored in this analysis.

Figure 16 shows the relationship between age and (B-R) colour from BC03 models used in the analysis. Overplotted on these points are our parametric fits between these two quantities. Colours above  $(B - R) = 0.75$  are fit to a log profile and colours equal to and below this value are fit to a straight line in order to reduce the degeneracy in low colour values. The form of these fits are shown below.

$$(B - R) = \begin{cases} 0.485 \log(\text{age}/\text{Gyr}) + 1.08, & (B - R) > 0.75 \\ 1.566(\text{age}/\text{Gyr}) + 0.033, & (B - R) \leq 0.75 \end{cases}$$

Each pixel is sorted by morphological type and the equivalent ages are calculated. The distribution of ages of each galaxy type are discussed in the next section.

The models are not well fit for the region around 5 Gyr. However, the relation is monotonic and we are interested in relative ages only. Therefore, the systematic offset introduced in this region does not present a problem for our purpose in this analysis.



**Figure 16.** Fitting the BC03 models, with a Chabrier IMF. Colours above  $(B - R) = 0.75$  were fit to a  $\log(x)$  profile whereas colours below this were fit as straight lines.

### 5.1 Age Distributions of Pixels

Figure 17 shows the distribution of ages for all pixels in our sample, sorted via morphological type. We see a clear separation in age for each galaxy type. We recognise that the difficulties of estimating ages with only two photometric bands means that the absolute ages stated here should not be taken literally. The comparison of the pixel colours with the BC03 models yield ages which are too low to comply with current age estimates, for example, of stellar populations in globular clusters (Sharina et al. 2006, Strader et al. 2005, Krauss & Chaboyer 2003). Rather, these results are more useful for looking at the relative ages of pixels in each galaxy type. One reason these fits give such young ages is due to the large degeneracy between age and colour after 6 Gyr.

The ellipticals appear to be the oldest, with the majority of their pixels having been formed significantly before those of all the other types. The S0 population appears to be the next oldest with a distribution similar to that of the mid-types but shifted in age. The distribution of the late-types, with fitted ages less than 1 Gyr, are so blue they fall into the very steepest region of the BC03 models (see Fig. 16).

However, there are inherent biases in this pixel analysis. Younger stars tend to be bluer and much brighter than older, redder stars and hence will have more influence on the measured colour of a pixel. Some pixels will also naturally contain more stars than others and will contribute more flux purely due to numbers. The former bias is impossible to fix but adjustments can be made for the latter by altering Fig. 17 to account for the amount of stellar mass in each pixel. This is carried out in the next section.

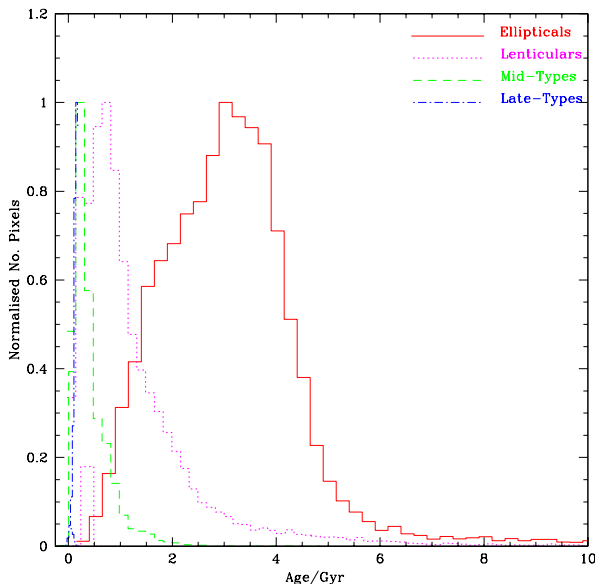


**Figure 17.** The age distribution of the pixels of all galaxies, sorted into morphological type. These ages were produced using the BC03 models assuming solar metallicity.

## 5.2 Mass-Weighted Age Distribution

The stellar mass in each pixel of the galaxy images is calculated using the Bell & deJong (2001) relation for the mass-to-light ratio of galaxies as a function of (B - R) colour, as listed in equation (2).

$$\log_{10}\left(\frac{M}{L}\right) = -1.224 + 1.251(B - R) \quad (2)$$

The total mass in each age bin is calculated and these values are normalised for each galaxy type. The normalised mass values are plotted against the mid-point of each age bin and the results are shown in Fig. 18. The effect of this mass-weighting is to increase the ages of some pixels. The peak age of the ellipticals, when weighted by mass, increases by approximately 0.5 Gyr, whereas the peak of the mid-types has now been increased to coincide with that of the S0s. All late-type pixels still fall at the lowest ages due to their very blue colours.

Interestingly, the effect of mass-weighting the S0s is to spread the age distribution. There is a trend of steady increase in total stellar mass up to  $\sim 1.5$  Gyr and then a rapid decline up to the present epoch. This is in contrast to the ellipticals, which seem to have a limited range in age, with little or no mass formation at the present epoch. This tail in the S0s suggests that many of their pixels are older than those of the ellipticals. However, this is not likely to be real, rather it results from some of the S0 pixels having very red (B-R) colours due to the presence of dust. This tail of old S0 pixels can be seen in Figure 15. The pixels that have these extreme red colours in the S0s are also some of the brightest, hence they become more pronounced in the mass-weighted age diagram.

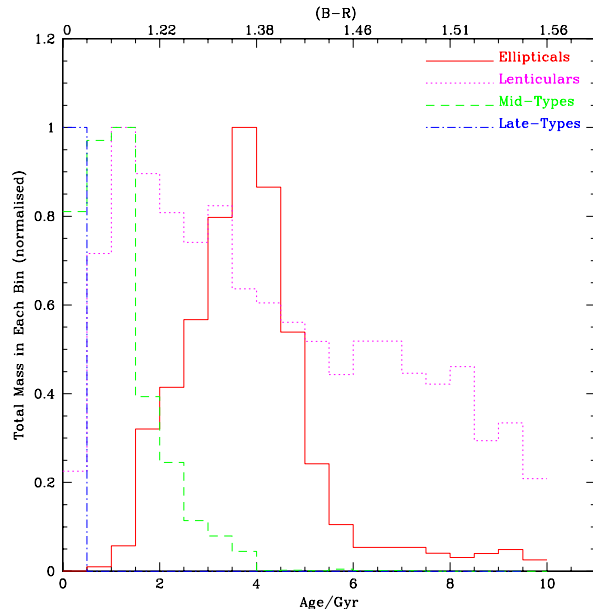


**Figure 18.** Mass-weighted age distribution of the pixels of all galaxies, sorted into morphological type. Stellar masses of each pixel were calculated using the Bell & DeJong (2001) model for calculating mass-to-light ratios for B and R band luminosities. The stellar masses of each pixel were then binned according to age and summed.

## 5.3 Stellar Population Maps

Pixel-by-pixel analysis allows us to investigate galaxy properties that cannot be probed using integrated light alone. Using the masses of each pixel, calculated in §5.2, we can construct maps of the stellar mass distribution and M/L ratio distribution throughout each galaxy. Figure 19 illustrates comparisons between galaxy images, stellar mass distributions and mass-to-light ratio maps for five galaxies representative of each morphological type. The scale of both the stellar mass and M/L maps is set such that the brighter pixels represent those with larger masses and higher M/L ratios. The masses and M/L maps are calculated with the negative pixel values removed. This is so that low S/N pixels in the images can still be mapped.

### 5.3.1 Stellar Mass Maps

In general for these example galaxies the stellar mass distributions follow the light in the images (Figure 19). The most massive pixels lie close to the centres of all galaxies. Spiral structure can still be identified in NGC 3368 although the mass distribution is smoother than that of the light, suggesting that concentrations of light do not always correspond to concentrations of mass. Star formation will dominate the galaxy image, as discussed in §5.1, but the mass appears to be more evenly spread throughout the disc. This is confirmed in the mass map of NGC 3631 where the spiral arms are not so prevalent, instead the mass of the disc is approximately constant throughout the disc, with the exception of a few small knots. The same is true of the irregular galaxy NGC 4449, whose mass distribution appears much smoother than the light in the optical image.

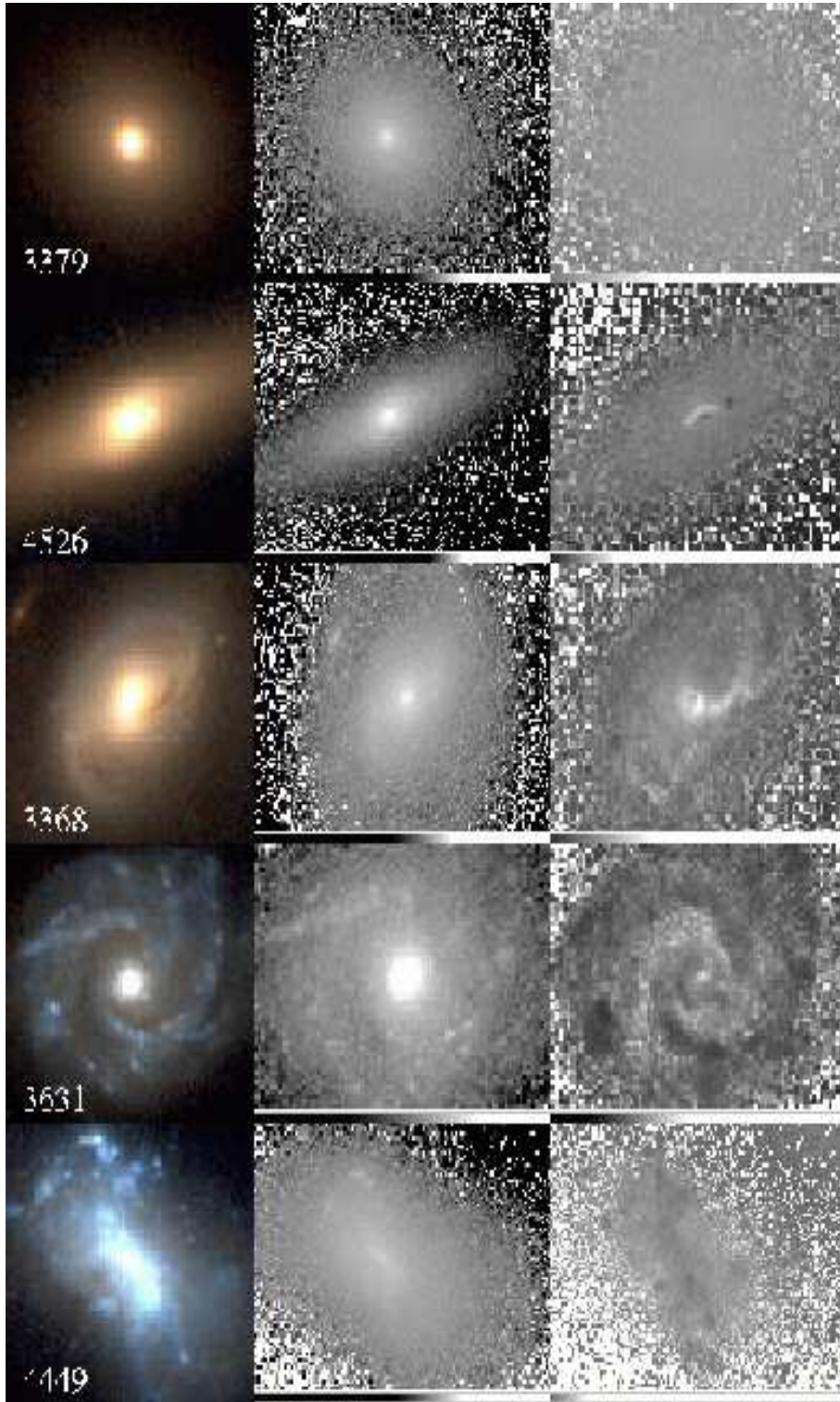


**Figure 19.** A comparison between the light, stellar mass and mass-to-light distributions of galaxies across the Hubble sequence, arranged from left to right. The brighter pixels indicate the greatest masses/highest mass-to-light ratios. The galaxies shown (from the top) are NGC3379 (E), NGC4526 (S0), NGC3368 (mid-type), NGC3631 (late-type) and NGC4449 (irregular).

### 5.3.2 *Mass-to-Light Ratio Maps*

The M/L ratio maps show more variation in their distributions than the stellar mass maps. We note that all pixels in the M/L ratio maps of NGC 3379 (E), NGC 4526 (S0) and

NGC 3368 (mid-type) have values of  $M/L > 1$ . However, for NGC 3631 (late-type) and NGC 4449 (irregular) all the pixels in the maps have values of M/L between 0 and 1. In all maps, the scale indicates that the brightest pixels have the highest values of M/L.

The M/L ratio is approximately constant in the early-type galaxies. Although the few highest valued pixels in the S0 lie in the central regions of the galaxy a central concentration has disappeared altogether in the elliptical. This implies that, while there is more mass than light throughout NGC 3379, the bright central pixels evident in the Frei image and the mass map are not only very massive, they are also very bright.

NGC 3368 yields an interesting M/L map (Fig. 19), displaying a bias in M/L ratio in one spiral arm. This is explained by the presence of dust on that side of the galaxy, as seen in the light image. This dustier, redder section of the galaxy will appear older and will appear to have a boosted M/L ratio for that reason.

Star formation dominates most of the pixels in the M/L maps of NGC 3631 and NGC 4449 such that the brightest pixels in the Frei image tend to have low M/L values. The bulge almost disappears in the map of NGC 3631 implying that the stars in this region are still relatively young although the spiral structure that was diminished in the mass map reappears in the M/L map.

## 6 APPLICATION TO THE UDF

For the pCMD technique to be truly useful as an analysis and classification tool, it must be transferable between photometric bands and redshifts. We test this condition by applying the method to the Hubble Ultra Deep Field (HUDF) in the  $i(775\text{nm})$  and  $z(850\text{nm})$  bands. One early-type galaxy and two spirals are chosen. The pCMDs are constructed from these images using the method described in §2. The resulting pCMDs are shown in Figure 20.

The early-type galaxy does not appear any redder in ( $i-z$ ) than the spirals, although its radial profile is more uniform and its gradient steeper. The spirals do not seem to show as much structure in their pCMDs as would be expected from the findings of §3. This could be due to the smaller difference in wavelength between  $i$  and  $z$  compared to the difference between the  $B$  and  $R$  bands in the Lowell sample. It could also be due to the different underlying stellar populations in the high- $z$  when compared with the local galaxies. The effects of “beam dilution” can be discounted in this instance as the typical scale subtended by a pixel in the HUDF galaxies chosen is of the order of that in the local sample. This is partially due to the much greater resolution of the ACS than the nearby galaxy images taken from the ground.

This exercise demonstrates that a pixel-by-pixel analysis can be performed over a wide range of redshifts and photometric bands.

## 7 DISCUSSION AND CONCLUSIONS

### 7.1 pCMDs

Pixel colour magnitude diagrams provide a novel way of looking at the stellar populations and structures of galaxies. We find that the pCMDs of each galaxy type are distinct and trends have been identified.

Elliptical pCMDs tend to have a small spread in colour throughout their radii and have nearly uniform, red colours,

which we call the “prime sequence”. The lenticular galaxies in the sample are similar to the elliptical pCMDs but with a greater internal colour spread. The mid and late-type pCMDs tend to be bluer than the E and S0s and have a greater colour gradient throughout their radius, such that they are bluer toward the edges of the galaxies and redder in the central regions. The mid and late-type pCMDs display more varied structures. Trends within these types are identified.

We find that “inverse-L” shape pCMDs correspond to face-on spiral galaxies and the distinct red and blue regions of the pCMDs are caused by the bulge and disc components of the galaxies. Dusty and high inclination spirals produce pCMDs with a large spread in colour throughout their radii and this could also explain the greater color spread of the lenticular pCMDs. Individual features of two galaxies are identified through their pCMDs. These are the optical jet in NGC4486 and a prominent dust lane in NGC4826. Red Hook features are identified in 6 early-type galaxies. These are attributed to dust in the central regions of the galaxies.

### 7.2 Pixel-by-Pixel Analysis

Pixel-by-pixel analysis is a useful way of gaining information from galaxy images and reveals information that analysis of integrated light does not. In this paper, we explore methods that can be used as part of an automated classification system for galaxies using pixels and define some new parameters, such as the blue-to-red light ratio.

We look at the internal colour distributions of galaxies in a new way. The colour distributions of all pixels are organised by morphological type and we find that these alone show no bimodality in colour within one type. We confirm that there does appear to be a steady progression in average pixel colour along the Hubble sequence, with late-types exhibiting the bluest colours and ellipticals the reddest, as expected.

We compare our galaxy pixel colours to the Bruzual & Charlot (2003) stellar population models and use this to calculate ages and mass-weighted ages for each pixel, organised by type. We find that elliptical galaxies have the oldest and late-types the youngest pixels.

The pixel-by-pixel technique allows the stellar mass distribution and M/L ratio in galaxies to be mapped. We find that the mass tends to follow the light in the cases of the five example galaxies tested. This is not the case with the M/L maps, which show trends related to both star formation and dust extinction. Pixel-by-pixel mass maps is a more fundamental way of looking at galaxies and it will be very interesting to apply to galaxies at high redshift.

### 7.3 Application to High- $z$ Galaxies

Finally, we create pCMDs for three galaxies in the HUDF in the  $i(775)$  and  $z(850)$  bands. This proves that the pCMD analysis can transcend different data sets, different bands and can be applied to galaxies at high redshift.

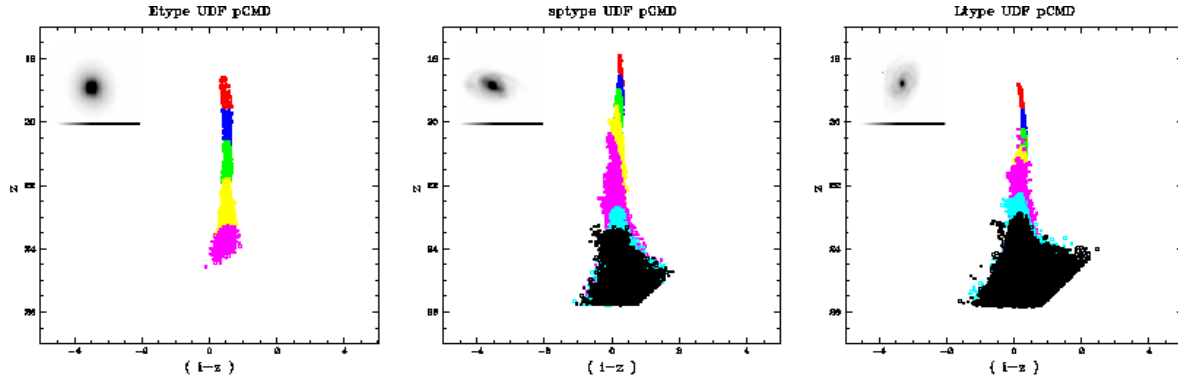


**Figure 20.** The pCMDs of 3 galaxies chosen from the UDF in the i and z bands.

#### 7.4 Future Work

There is much more that can be done using a pixel approach to analysing galaxy image data. This work presents new questions about the morphological evolution of galaxies that need to be answered. For example, further investigation of the central regions of nearby early-type galaxies is needed to explore the origins of the Red Hooks.

An in-depth analysis of individual galaxies would be very interesting using a pixel approach, as an extension to this and previous work by Bothun (1986) and Eskridge et al. (2003). For example, looking at HST data of nearby galaxies, such as M51, could allow for a pCMD that reveals further features that integrated light analyses cannot.

The pixel approach could be further exploited by formulating new structural parameters of galaxies. This would be an extension of the CAS system introduced by Conselice, Bershady and Jangren (Conselice et al., 2000, Bershady et al., 2000) where parameters are calculated pixel-by-pixel instead of through the use of light profiles, etc. In combination with the further development of stellar mass maps and their application to high redshift galaxies, a pixel approach will provide a more fundamental way of investigating and classifying galaxies.

#### ACKNOWLEDGMENTS

We would like to thank Reynier Peletier for useful communications about the nature of the centres of early-type galaxies. We would also like to thank the referee for their very helpful comments and suggestions. MML acknowledges postgraduate funding from the Particle Physics and Astronomy Research Council (UK).

#### REFERENCES

- Abraham, R.G., et al. 1996, ApJS, 107, 1  
 Abraham, R.G., et al. 1999, MNRAS, 303, 641  
 Bell, E.F. & de Jong, R.S., 2001, ApJ, 550, 212B  
 Bershady, M.A., Jangren, J.A., & Conselice, C.J. 2000, AJ, 119, 2645  
 Binney, J. & Merrifield, M. R., 1998, Galactic Astronomy (Princeton: Princeton University Press)  
 Bothun, G.D., 1986, AJ, 91, 507  
 Bothun, G.D. & Gregg, M. D., 1990, ApJ, 350, 73  
 Bridge, C., et al. astro-ph/0701040  
 Bruzual, G. & Charlot, S. 2003, MNRAS, 344, 1000  
 Bundy, K., Ellis, R., Conselice, C., 2005, ApJ, 625, 621  
 Cassata, P., et al. 2005, MNRAS, 357, 903  
 Conselice, C.J., Bershady, M.A., & Jangren, A. 2000, ApJ, 529, 886  
 Conselice, C.J. 2003, ApJS, 147, 1  
 Conselice, C.J. et al., 2003, AJ, 126, 1183  
 Conselice, C.J., Blackburn, J. A., Papovich, C., 2005, ApJ, 620, 564  
 Conselice, C. 2006, ApJ, 638, 686  
 Conselice, C. 2006b, MNRAS, 373, 1389  
 de Vaucouleurs, G. 1959, Handb. der Physik, 53, 275  
 Driver, S., Windhorst, R.A. & Griffiths, R.E. 1995, ApJ, 453, 48  
 Driver, S., et al. 1998, ApJ, 496, L93  
 Driver, S.P., et al. 2006, MNRAS, 368, 414  
 Elmegreen, D.M. & Elmegreen, B.G. 1982, MNRAS, 201, 1021  
 Elmegreen, D.M. & Elmegreen, B.G. 1987, ApJ, 314, 3  
 Eskridge, P.B., et al. 2003, ApJ, 586, 923  
 Frei, Z., Guhathakurta, P., Gunn, J.E. & Tyson, J.A. 1996, AJ, 111, 174  
 Hubble, E. 1926, ApJ, 64, 321  
 Hubble, E. 1936, The Realm of the Nebulae, (New Haven: Yale University Press)  
 Krauss, L.M. & Chaboyer, B., 2003, Sci, 299, 65  
 Lauer, T., et al. 2005, AJ, 129, 2138  
 Lin, L., et al. 2004, ApJ, 617, 9L  
 Lotz, J., et al. 2006, astro-ph/0602088  
 Morgan, W.W. 1958, PASP, 70, 364  
 Morgan, W.W. 1959, PASP, 71, 394  
 Roberts & Haynes, ARA&A, 32, 115  
 Sandage, A. 1961, The Hubble Atlas of Galaxies (Washington, DC: Carnegie Institution of Washington)  
 Sharina, M.E., Afanasiev, V.L. & Puzia, T.H., 2006, MNRAS, 372, 1259  
 Strader, J., et al. 2005, AJ, 130, 1315  
 van den Bergh, S. 1960, Publ. David Dunlap Obs., 2, 159  
 van den Bergh, S. 1995, AJ, 110, 613